the FEBS Journal

Insights into the slow-onset tight-binding inhibition of *Escherichia coli* dihydrofolate reductase: detailed mechanistic characterization of pyrrolo [3,2-*f*] quinazoline-1,3-diamine and its derivatives as novel tight-binding inhibitors

Bharath Srinivasan and Jeffrey Skolnick

Center for the Study of Systems Biology, Georgia Institute of Technology, Atlanta, GA, USA

Keywords
dihydrofolate reductase; drug discovery; mechanistic characterization; pyrrolo [3,2-*f*] quinazoline-1,3-diamine; slow–tight-binding inhibition

Correspondence
J. Skolnick, Center for the Study of Systems Biology, School of Biology, Georgia Institute of Technology, 250, 14th Street, NW, Atlanta, GA 30318, USA
Fax: +1 404 385 7478
Tel: +1 404 407 8975
E-mail: skolnick@gatech.edu

(Received 13 November 2014, revised 13 February 2015, accepted 17 February 2015)

doi:10.1111/febs.13244

Dihydrofolate reductase (DHFR) is a pivotal enzyme involved in the *de novo* pathway of purine synthesis, and hence, represents an attractive target to disrupt systems that require rapid DNA turnover. The enzyme acquires resistance to available drugs by various molecular mechanisms, which necessitates the continuous discovery of novel antifolates. Previously, we identified a set of novel molecules that showed binding to *E. coli* DHFR by means of a thermal shift without establishing whether they inhibited the enzyme. Here, we show that a fraction of those molecules represent potent and novel inhibitors of DHFR activity. 7-[(4-aminophenyl) methyl]-7H-pyrrolo [3,2-*f*] quinazoline-1,3-diamine, a molecule with no reported inhibition of DHFR, potently inhibits the enzyme with a K_i value of 7.42 ± 0.92 nM by competitive displacement of the substrate dihydrofolic acid. It shows uncompetitive inhibition vis-à-vis NADPH, indicating that the inhibitor has markedly increased affinity for the NADPH-bound form of the enzyme. Further, we demonstrate that the mode of binding of the inhibitor to the enzyme–NADPH binary complex conforms to the slow-onset, tight-binding model. By contrast, mechanistic characterization of the parent molecule 7H-pyrrolo [3,2-*f*] quinazoline-1,3-diamine shows that lack of (4-aminophenyl)-methyl group at the seventh position abolishes the slow onset of inhibition. This finding provides novel insights into the role of substitutions on inhibitors of *E. coli* DHFR and represents the first detailed kinetic investigation of a novel diaminopyrrolo-quinazoline derivative on a prokaryotic DHFR. Furthermore, marked differences in the potency of inhibition for *E. coli* and human DHFR makes this molecule a promising candidate for development as an antibiotic.

Introduction

Dihydrofolate reductase (DHFR, EC 1.5.1.3) is a ubiquitous enzyme found in all kingdoms of life. The enzyme is involved in the reduction of 7,8-dihydrofolate (H_2F) to 5,6,7,8-tetrahydrofolate (H_4F) during which protonation of H_2F on N5 precedes the hydride transfer from C4 of the NADPH cofactor to the C6 atom of the pterin ring on H_2F [1]. Since DHFR is the sole source of cellular tetrahydrofolate, a metabolite

Abbreviations
AMPQD, 7-[(4-aminophenyl) methyl]-7H-pyrrolo [3,2-*f*] quinazoline-1,3-diamine; DHFR, dihydrofolate reductase; H_2F, 7,8-dihydrofolate; H_4F, 5,6,7,8-tetrahydrofolate; MTX, methotrexate; PQD, 7H-pyrrolo [3,2-*f*] quinazoline-1,3-diamine.

essential for thymidylate and purine synthesis, its activity is indispensable. Thus, the enzyme represents an attractive target to disrupt systems that require rapid DNA turnover, e.g. proliferating cancer cells and pathogenic microbes [2]. *Escherichia coli* DHFR has been extensively characterized in terms of kinetic mechanism, catalysis and structural studies [3–6]. This wealth of data makes the enzyme an attractive target for the design of small-molecule inhibitors as potential antibiotics. This has become all the more important given the increase in instances of nosocomial infection caused by drug-resistant *E. coli* [7]. However, designing inhibitors for DHFR presents considerable challenges because the enzyme acquires rapid resistance to available drugs by means of gene amplification, mutations and decreased drug uptake [8].

A lot of effort has been expended on discovering novel inhibitors for DHFR from different organisms, given their potential applications to antineoplastic, anti-inflammatory and anti-infective drug discovery [9–11]. Methotrexate (MTX), a 2,4-diaminopteridin, is by far the most well characterized inhibitor of DHFR, showing a slightly increased potency of inhibition for parasitic DHFR compared to either human or bacterial DHFR. Other prominent antifolates include the pyrimidine-2,4-diamine pyrimethamine, which is highly specific for eukaryotic DHFRs, trimethoprim, which shows a slightly greater preference for prokaryotic DHFRs [2], metoprine and piritrexim. Further, to overcome the limitation imposed by the hydrophilic nature of MTX, which hinders its distribution across different tissues, lipophilic inhibitors like trimetrexate, a quinazoline-2,4-diamine, have been synthesized as nonclassical inhibitors of DHFRs. Pyrrolo [3,2-*f*] quinazoline-1,3-diamine derivatives, containing a novel tricyclic heterocycle compared with trimetrexate, were further explored and shown to be inhibitors of parasitic DHFRs [12]. Other studies have shown 7,8-dialkyl-1,3-diaminopyrrolo [3,2-*f*] quinazoline compounds to be high-affinity inhibitors of DHFR from *Pneumocystis carinii* and *Candida albicans* [13]. In yet another study, a high-throughput screen identified 12 compounds as inhibitors of *E. coli* DHFR [14]. However, it should be noted that detailed kinetic studies on the inhibition brought about by these novel DHFR inhibitors is lacking.

Previously, as part of experimental validation of the virtual ligand-screening algorithm FINDSITE^{comb} and relying on thermal-shift assay methodology, we reported a set of novel molecules that showed binding to *E. coli* DHFR [15,16]. Here, employing inhibition kinetics, we show that a fraction of those molecules represent novel inhibitors of DHFR activity and present detailed mechanistic characterization to substantiate our claims. By means of extensive steady-state and tight inhibition kinetics studies, we show for the first time that 7-[(4-aminophenyl) methyl]-7H-pyrrolo [3,2-*f*] quinazoline-1,3-diamine (AMPQD) and its parent compound, 7H-pyrrolo [3,2-*f*] quinazoline-1,3-diamine (PQD), are novel tight-binding inhibitors of *E. coli* DHFR. These inhibitors preferentially bind to the NADPH-bound form of the enzyme at the H_2F-binding site. Although AMPQD shows slow onset of binding to the enzyme, PQD shows no such behavior, implicating the (4-aminophenyl) methyl group as a possible origin of the slow binding behavior in *E. coli* DHFR. This, combined with our already reported antibacterial, antifungal and antineoplastic activity by these compounds against two different strains of *E. coli* (multidrug-resistant *E. coli* and DH5α), a strain of methicillin-resistant *Staphylococcus aureus*, a strain of vancomycin-resistant *Enterococcus faecalis*, a strain of amphotericin B-resistant *C. albicans* and HCT-116 human colon carcinoma cell line, makes these compounds potential lead candidates to target conditions arising from aberrant DHFR activity [15]. Further, pronounced differences in the potency of inhibition and the mode of inhibitor binding for AMPQD and PQD against *E. coli* and human DHFR make these molecules attractive candidates for development as novel antibiotics.

Results

Inhibition of *E. coli* DHFR

All the hits from the FINDSITE^{comb} experimental validation study were assessed for their ability to inhibit *E. coli* DHFR. The histogram in Fig. 1 summarizes the results. All the reported inhibitors of DHFR from various sources, viz. MTX (NSC740), PQD (NSC 339578), methylbenzoprim (NSC382035), pralatrexate (NSC754230), pemetrexed (NSC698037) and 6,7-bis(4-aminophenyl) pteridine-2,4-diamine (NSC61642), show unambiguous inhibition of *E. coli* DHFR at a 1 mM inhibitor concentration. Prior to carrying out IC_{50} determination and detailed inhibition studies, the kinetic parameters for the substrate H_2F and cofactor NADPH were determined and found to be in agreement with values reported in the literature within experimental error (Table S1 and Fig. S1) [17,18]. For all further experiments, except when a substrate is titrated, the substrates were kept at > 10 times their respective K_m values. Table 1 and Fig. S2(A,B) summarize the IC_{50} values, defined as the concentration of inhibitor required to reduce the activity of the enzyme

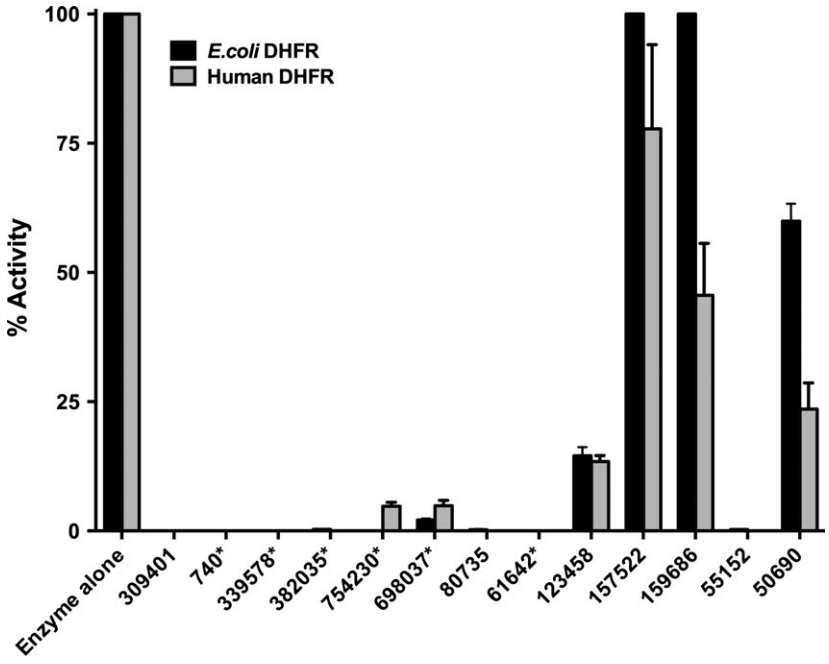

Fig. 1. Comparative inhibition of DHFR from *E. coli* and humans. Each histogram represents the activity of *E. coli* (black) or human DHFR (gray) in the presence of the inhibitor molecules tested at a fixed concentration of 1 mM. All activities are expressed as percentage activity with respect to the enzyme control for ease of comparison across the two enzymes. The numbered notations for the various inhibitor molecules represent NSC numbers. The numbers with an asterisk represent molecules that have been previously reported as having DHFR inhibitory activity from various organisms and independently 'predicted' by our method.

by 50%, determined for a select set of reported inhibitors of *E. coli* DHFR independently identified by our studies.

Among the nine novel binders reported previously, seven were tested for their inhibition of *E. coli* DHFR [15]. Three (NSC309401, NSC80735 and NSC55152) showed almost complete inhibition and one molecule (NSC123458) showed ~ 87% inhibition at a 1 mM inhibitor concentration (Fig. 1). While NSC309401 (AMPQD) is a substrate analogue with the quinazoline-1,3-diamine group, NSC80735 and NSC55152 contain concatenated nitrophenyl and aminophenyl groups. To further understand their inhibition, IC_{50} values were determined for the various molecules. Figure 2A shows the curve of log inhibitor concentration versus activity for AMPQD, giving an IC_{50} value of 189.0 ± 1.0 nM (Table 1). This indicates potent inhibition comparable to that shown by MTX, with an IC_{50} value of 152.5 ± 1.1 nM. However, since it is known from the literature that IC_{50} values are enzyme concentration dependent and can never be $< [E_0]/2$ [19], it is highly likely that the number represents an underestimation of the actual affinity of the inhibitor for the enzyme (Fig. 2B).

Table 1. IC-50 and K_{iapp} values for various small molecule inhibitors of *E. coli* and human DHFR.

	E. coli DHFR		Human DHFR	
Small molecule[c]/NSC ID	IC-50 (nM)	K_{iapp}[a] (nM)	IC-50 (nM)	K_{iapp}[a] (nM)
AMPQD/NSC309401	189.0 ± 1.0	7.8 ± 0.8	599.0 ± 7.2	19.4 ± 2.7
PQD[b]/NSC339578	106.1 ± 1.2	4.2 ± 0.5	3087.1 ± 16.5	93.4 ± 9.0
MTX[b]/NSC740	152.5 ± 1.1	6.7 ± 0.7	147.7 ± 2.3	5.1 ± 1.0
NNCPPU/NSC80735	36560 ± 1100	2062 ± 378	68870 ± 1356	1973 ± 329
NNBABD/NSC55152	176500 ± 1114	10941 ± 2156	254500 ± 1789	5161 ± 1411
ISB/NSC123458	587800 ± 1184	35222 ± 5358	ND	ND

ND, not determined since it was greater than 2 mM.

[a] K_{iapp} was estimated by employing the Morrison equation. This equation accounts for tight binding, and hence does not assume that the free concentration of inhibitor equals the total concentration.

[b] Reported inhibitors of DHFR from various organisms independently identified by our method as inhibitors of human and *E. coli* DHFR.

[c] AMPQD, 7-[(4-aminophenyl)methyl]-7HPyrrolo[3,2-f]quinazoline-1,3-diamine; PQD, 7H-Pyrrolo(3,2-f)quinazoline-1,3-diamine; MTX, Methotrexate; NNCPPU, 1-(4-nitrophenyl)-3-[4-[4-[(4-nitrophenyl) carbamoylamino] phenoxy]phenyl]urea; NNBABD, N,N′-bis(4-aminophenyl)benzene-1,4-dicarboxamide; ISB, 2,2′-Iminostilbene.

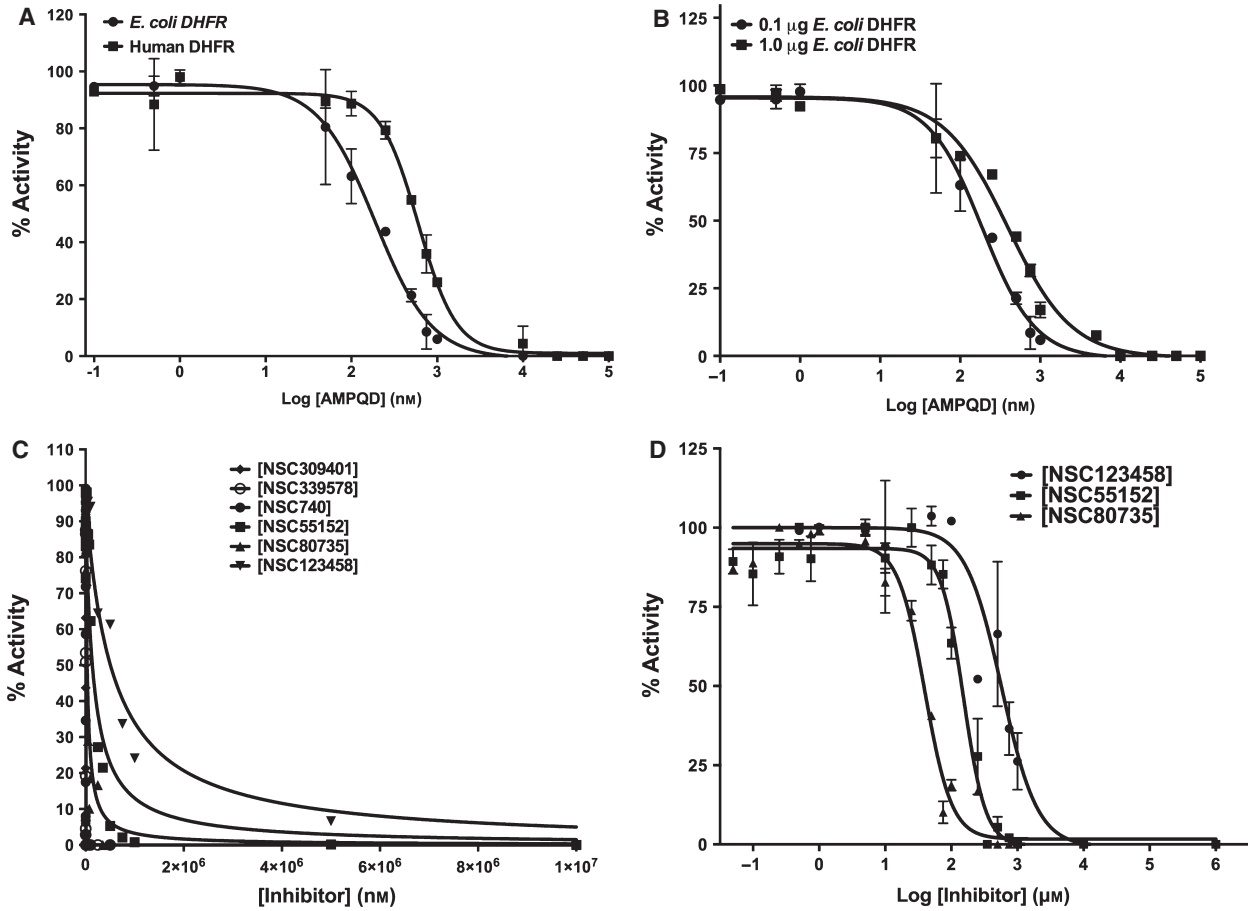

Fig. 2. Potency of inhibition. (A) IC_{50} determination for AMPQD against *E. coli* and human DHFR. (B) Enzyme concentration dependence of IC_{50} for the tight-binding inhibitor AMPQD for *E. coli* DHFR. (C) Fit of the experimental dose–response curves to Morrison's equation for tight binding for inhibitors of *E. coli* DHFR. (D) IC_{50} value estimates for inhibitors of *E. coli* DHFR not displaying tight-binding behavior (NSC80735, NSC55152 and NSC123458). On the plots, the *y*-axis represents % activity of the enzyme and the *x*-axis represents the log inhibitor concentration/inhibitor concentration. The experimental data points were fitted to the respective equations using the nonlinear curve-fitting algorithm of GraphPad PRISM v. 6.0e.

To account for this tight binding inhibition, the data were analyzed as per the methods developed by Morrison and coworkers [20,21]. Figure 2C shows the fit of the data to the quadratic Morrison equation for tight binding and Table 1 lists the K_{iapp} values computed from nonlinear curve fitting. As expected, the K_{iapp} value of 7.8 ± 0.8 nM for AMPQD is almost 25-fold lower than its IC_{50}. Further, compounds NSC80735, NSC55152 and NSC123458 were also titrated, and plots of their log inhibitor concentration versus activity yielded IC_{50} values of 36.56 ± 1.1μM, 176.5 ± 1.1 μM and 587.8 ± 1.2 μM, respectively (Fig. 2D and Table 1). However, because these three compounds are sparsely soluble in water, the reported IC_{50} values may, at most, represent gross approximations. Moreover, their high IC_{50} values and relative insolubility may lead to potential problems of bioavailability. Hence, these compounds may not represent promising lead candidates. It is worthwhile to point out that compounds NSC80735 and NSC55152 did not show either bactericidal activity or activity against cancer cells, as reported in our previous study [15]. Detailed mechanistic characterization was undertaken on AMPQD (the best hit from the FINDSITE^{comb} study), PQD (the parent molecule of AMPQD) and MTX (a well characterized DHFR inhibitor) to understand their mode of inhibition (Fig. 3).

AMPQD (NSC309401) is a competitive inhibitor of dihydrofolate binding

To further understand the inhibition shown by AMPQD, we resorted to detailed inhibition kinetics. Substrate dihydrofolate was titrated at several fixed

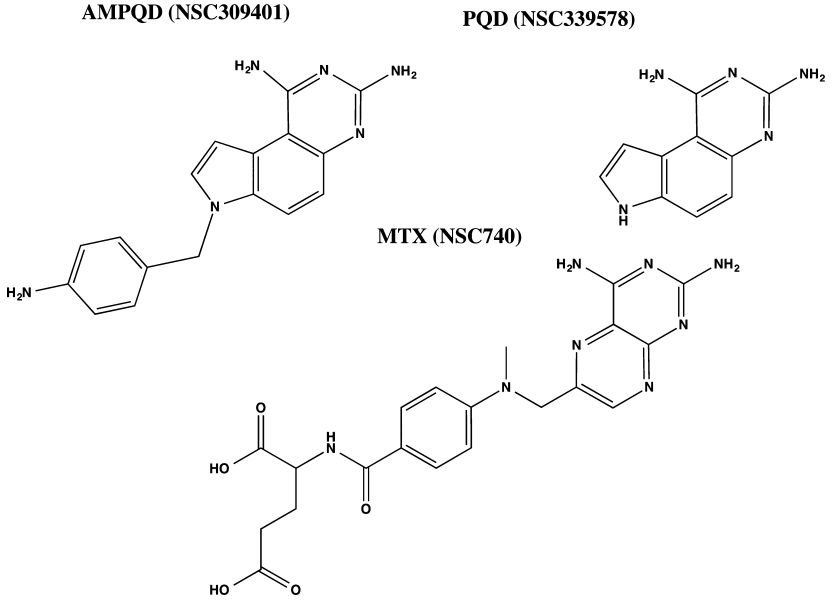

Fig. 3. Structures of (A) AMPQD (NSC309401), (B) PQD (NSC339578) and (C) MTX (NSC740). The SDF files for the structures were downloaded from PubChem database and the figures were made in CHEMBIODRAW 14.0.

concentrations of AMPQD, and the resulting curves from the primary plot, when globally fit to models for the various types of inhibition, showed the best fit to the model for competitive inhibition (see Experimental Procedures for details) (Fig. 4A) yielding a K_i, the equilibrium dissociation constant for the competitive inhibitor, of 7.42 ± 0.92 nM (Table 2). Further, for visual assessment, the data were transformed and plotted as the double-reciprocal Lineweaver–Burk plot. Figure 4B shows the lines of the Lineweaver–Burk plot intersecting on the *y*-axis, which is further indicative of competitive displacement of substrate dihydrofolate by AMPQD, whereby it increases the apparent K_m value for the substrate without unduly affecting the V_{max}. Further, this low K_i value, similar to that obtained from fitting to the Morrison equation, reinforces the fact that AMPQD is a tight-binding inhibitor, a special case in which the affinity of the inhibitor for the enzyme is an order-of-magnitude lower than the minimum concentration of enzyme that can be employed in the assay mix to obtain reliable activity. Further, the K_i value is ~ 25-fold lower than the obtained IC_{50}. However, the K_i value for AMPQD is approximately twofold higher than that reported for MTX (the reported value is ~ 3.6 nM) [22]. The above data are conclusive about AMPDQ binding to the same site as dihydrofolate and competing with the latter for high-affinity interactions with the enzyme. This competitive displacement can be ascribed to the quinazoline-1,3-diamine group shared by the two molecules (substrate and inhibitor), which might serve as the common motif responsible for binding. Although this behavior is similar to that shown by MTX, it is markedly different from that of a pyrimidine-2,4-diamine pyrimethamine against *Plasmodium* DHFR, which is a noncompetitive inhibitor of the latter [23].

AMPQD (NSC309401) is an uncompetitive inhibitor of NADPH binding

To understand the effect of AMPQD on the cofactor NADPH binding, the latter was titrated at several fixed concentrations of AMPQD, and the resulting curves from the primary plot, when globally fit to models for the various types of inhibition, showed the best fit to the model for uncompetitive inhibition (Fig. 4C) yielding an αK_i, the equilibrium dissociation constant for the uncompetitive inhibitor, of 162.9 ± 9.1 nM (Table 2). This higher αK_i value shows that the AMPQD binding site is fully formed only when the enzyme is bound to NADPH. It is worthwhile to point out that AMPQD K_i was ~ 7.4 nM at saturating NADPH (see above). Further, for visual assessment, the resulting data were transformed and plotted as the double-reciprocal Lineweaver–Burk plot. Figure 4D shows parallel lines on the Lineweaver–Burk plot, confirming the fit of primary data to model for uncompetitive inhibition. Data on the competition of AMPQD with NADPH are strongly indicative of an ordered binding event, whereby NADPH binding facilitates inhibitor binding. It should be noted that this pattern of uncompetitive inhibition against NADPH is similar to the way MTX behaves (Fig. S3A,B).

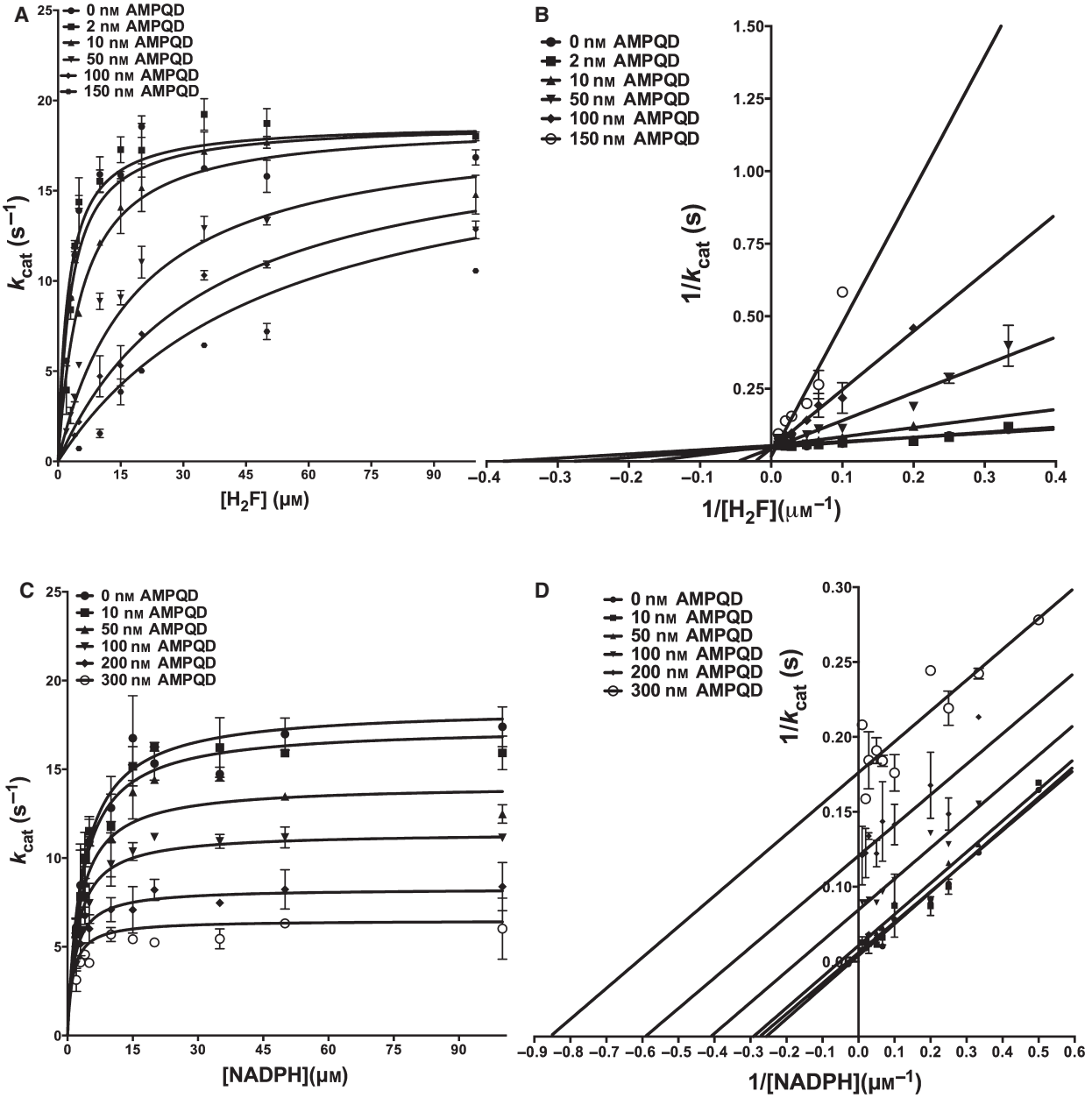

Fig. 4. Inhibition kinetics of AMPQD (NSC309401) for *E. coli* DHFR. (A) Fit of the primary data to the competitive inhibition model for H_2F titration at several fixed concentrations of AMPQD. (B) Double-reciprocal Lineweaver–Burk plot of H_2F titration at several fixed concentrations of AMPQD. (C) Fit of the primary data to the uncompetitive inhibition model for NADPH titration at several fixed concentrations of AMPQD. (D) Double-reciprocal Lineweaver–Burk plot of NADPH titration at several fixed concentrations of AMPQD. The *y*-axis shows the k_{cat} value. The experimental data points were fit to the respective models using the nonlinear curve-fitting algorithm of GraphPad PRISM v. 6.0e.

Although, in principle, *E. coli* DHFR can bind to both NADPH and H_2F randomly, as shown by some studies [6], productive catalysis proceeds through ordered ternary complex formation with NADPH binding prior to dihydrofolate. Furthermore, the pattern is also consistent with the pH-independent and pH-dependent models of the *E. coli* DHFR kinetic mechanism proposed by Fierke *et al.* [4], which show that dihydrofolate always binds to the NADPH-bound form of the enzyme. In a previous study, we have shown that AMPQD independently binds to the enzyme in the absence of NADPH [15]. Hence, the

Table 2. Parameters from inhibition kinetics and time-dependent inactivation of *E. coli* DHFR.

Inhibitors	Substrate	Inhibition	K_i /αK_i (nM)[a]	k_{off} (min^{-1})	k_{on} ($nM^{-1}\cdot min^{-1}$)	K_D (nM)
AMPQD	H_2F	C	7.42 ± 0.92	0.118 ± 0.017	0.008 ± 0.001	14.57 ± 2.10
	NADPH	U	162.70 ± 9.06	NA	NA	NA
PQD	H_2F	C	3.18 ± 0.51	0.094 ± 0.010	0.021 ± 0.002	4.48 ± 0.63
	NADPH	U	72.17 ± 4.23	NA	NA	NA
MTX	H_2F	C	3.6[b]	0.223 ± 0.078	0.013 ± 0.004	17.15 ± 2.92
	NADPH	U	111.00 ± 7.32	NA	NA	NA

C, competitive inhibition; U, uncompetitive inhibition.
[a] The K_i reported is for competitive inhibition while αK_i is reported for uncompetitive inhibition; K_D represents k_{off}/k_{on}; NA, not applicable.
[b] The value reported is from the study [21].

type of inhibition should ideally be either noncompetitive or linear mixed-type. However, the difference between K_i and αK_i is large. Hence, for all practical purposes, this inhibition can be considered uncompetitive. Thermal-shift assay measurements carried out from 0 to 500 nM AMPQD in the absence of NADPH were unsuccessful in stabilizing the protein and showed preferential binding to the denatured form of the protein. However, at a high concentration of 1 mM, the inhibitor showed binding to the enzyme, even in the absence of added NADPH, as seen in the thermal stability profile (Fig. S4). This further proves that AMPQD binding in the nM concentration range is absolutely conditional upon NADPH binding to the enzyme.

PQD inhibition kinetics

PQD has been shown to possess inhibitory activity against DHFRs from eukaryotic sources, inhibiting fungal DHFRs [13]. In order to assess its inhibition of a prokaryotic enzyme, it was tested against *E. coli* DHFR (Fig. 1 and Fig. S2A). PQD is the parent molecule for AMPQD and lacks the latter's (4-aminophenyl) methyl group. Figure 5A,B shows the primary curves for H_2F titration at several different concentrations of PQD fit to the model of competitive inhibition and the double-reciprocal Lineweaver–Burk plot. Further, Fig. 5C,D shows the primary curves for NADPH titration at several different concentrations of PQD fit to the model for uncompetitive inhibition and the double reciprocal Lineweaver–Burk plot. These patterns show that PQD occupies the H_2F binding site and preferentially binds to the NADPH-bound form of the enzyme, mirroring the behavior shown by its derivative AMPQD. However, the K_i value of 3.18 ± 0.51 nM for PQD is approximately half of that shown by AMPQD, indicative of tighter binding (Table 2).

In an attempt to rationalize the ordered binding behavior, whereby all three inhibitors preferentially bind to the NADPH-bound binary complex of the enzyme, structures of *E. coli* DHFR in complex with NADPH (PDB ID: 1RX1) and MTX (PDB ID: 3DRC) were analyzed. When the structures were superimposed with their respective ligands, maximum change was noticed in the M20 loop that covers the active site where the hydride transfer reaction from NADPH to H_2F happens (Fig. 6A). Furthermore, it became clear that the dramatic change in the orientation of M20 from the MTX-bound form to NADPH-bound form of the enzyme might be the principal reason of why the inhibitors prefer the NADPH form (Fig. 6A,B). This shift in the orientation between the two structures makes the thio group of methionine come within hydrogen-bonding distance of the N8 group on MTX in the NADPH-bound structure. Since AMPQD shares this substructure with MTX, it is highly likely that this interaction with M20 increases the affinity of the inhibitor for the enzyme manifold. Further, apart from this principal interaction, the whole M20 loop with several charged and bulky residues undergoes a change between the two structures. Other residues that may have possible roles in this preferential binding of inhibitor to NADPH-bound form are M16 and E17.

Slow-onset tight-binding inhibition: comparative study between AMPQD and PQD

AMPQD and PQD bind to *E. coli* DHFR with the same kinetic behavior as the well-characterized inhibitor MTX. Both are competitive with respect to H_2F and show preferential binding to the NADPH-bound form. Since it is known that MTX shows a slow-onset tight-binding mode to the enzyme [22], we wanted to ascertain whether this also holds true for AMPQD and PQD. The K_{iapp} values obtained for both AMPQD and PQD using steady-state methods show that the inhibitors are tight-binding inhibitors (Table 1). Progress curve analysis was used to determine whether

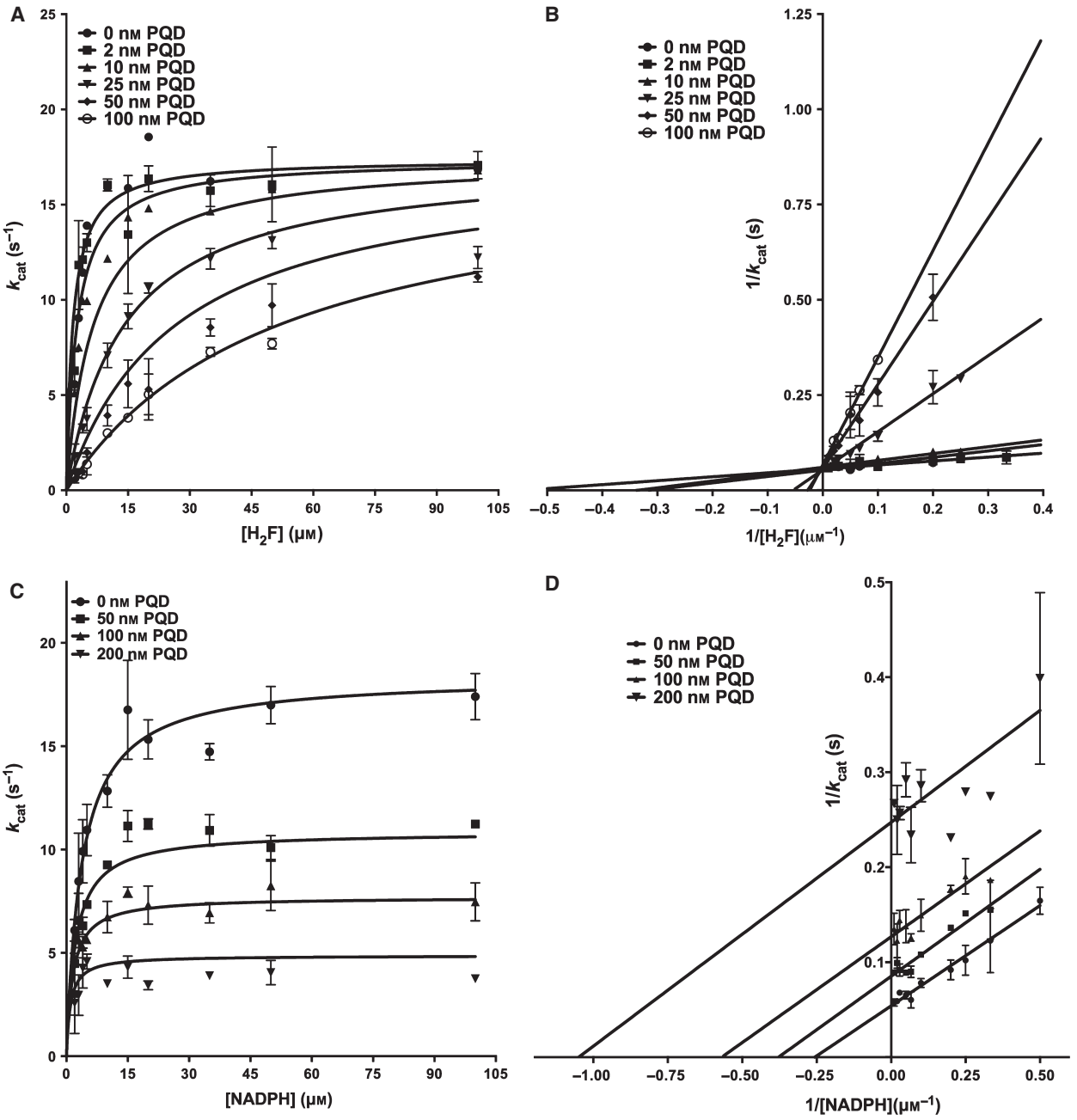

Fig. 5. Inhibition kinetics of PQD (NSC339578) for *E. coli* DHFR. (A) Fit of the primary data to the competitive inhibition model for H_2F titration at several fixed concentrations of PQD. (B) Double-reciprocal Lineweaver–Burk plot of H_2F titration at several fixed concentrations of PQD. (C) Fit of the primary data to the uncompetitive inhibition model for NADPH titration at several fixed concentrations of PQD. (D) Double-reciprocal Lineweaver–Burk plot of NADPH titration at several fixed concentrations of PQD. The *y*-axis shows the k_{cat} value. The experimental data points were fit to the respective models using the nonlinear curve-fitting algorithm of GraphPad PRISM v. 6.0e.

the inhibitors showed slow-onset of tight binding in inhibiting *E. coli* DHFR. Upon addition of AMPQD, the rate of product formation decreased exponentially with time from an initial velocity (v_i) to a steady-state velocity (v_s) (Fig. 7A). In addition, v_i, v_s and the time required to reach v_s decreased with increasing concentrations of the inhibitor, whereas k_{obs} increased (Fig. 7A inset). This nonlinear behavior in product formation in the presence of inhibitor complies with both the simple reversible slow-onset tight-binding

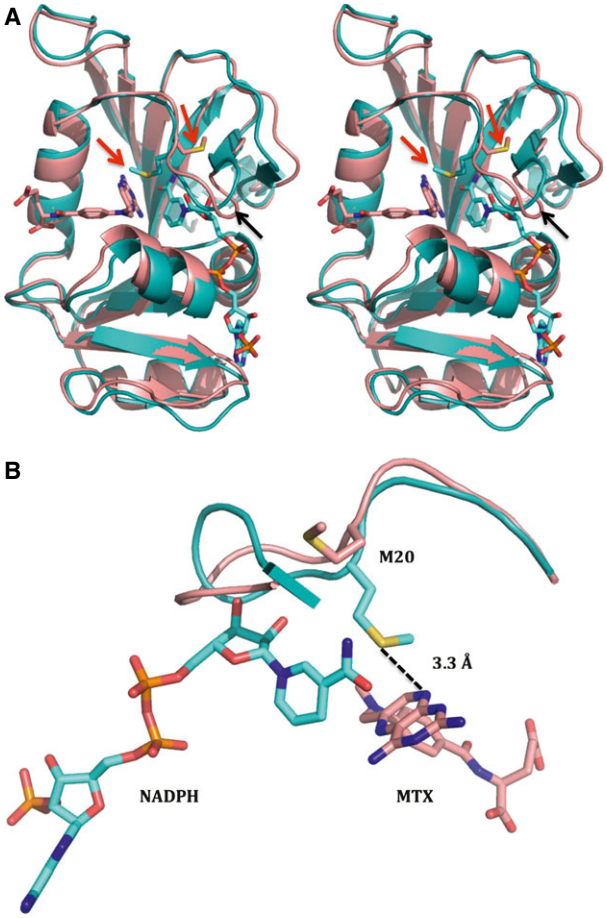

Fig. 6. (A) Stereo image of the superimposed cartoon representation for NADPH-bound (PDB ID: 1RX1) and MTX-bound (PDB ID: 3DRC) *E. coli* DHFR highlighting the movement of M20 loop. The NADPH-bound structure is shown in teal, the MTX-bound structure is shown in salmon, and the ligands are shown in a stick representation in the respective colors. The red arrows indicate the position of the flipped methionine 20 and the black arrows show the movement of M20 loop upon NADPH binding. (B) Zoomed-in representation highlighting the almost 180° flip of the methionine side chain in NADPH-bound *E. coli* DHFR that brings the thio group of methionine within hydrogen-bonding distance of the N8 group of MTX. The hydrogen bonds are shown in dotted representation. The figures were generated with MACPYMOL.

inhibition model and inhibitor binding followed by isomerization model. However, upon assessing the effect of preincubation time with inhibitor on the steady-state velocity of the reaction, whereby v/v_i was plotted against time at various fixed inhibitor concentrations, the behavior conformed to the classic reversible slow-onset inhibition in which no isomerization happens after rapid formation of the initial E–I complex (data not shown). A simple reversible equilibrium between the enzyme and inhibitor with association and dissociation rate constants k_3 and k_{-3}, respectively, defines this model aptly, as shown in Scheme 1. This behavior is similar to that of any reversible inhibitor, except that the values of k_3 and/or k_{-3} are smaller, leading to the slow-onset of inhibition. Further, as can be seen in the inset to Fig. 7A, the increase in k_{obs} is linear with respect to inhibitor concentration, conforming to the mechanism of reversible slow binding with slope equal to k_3 and y-intercept equal to k_{-3}. However, it should be noted that the measured value of k_3 is apparent, because this rate constant is substrate concentration dependent, as is seen in the plot of v_i versus AMPQD at several fixed concentrations of H_2F (Fig. 7B). Hence, the apparent value of K_i (K_{iapp}) for an inhibitor of this type can be calculated from the ratio of k_{-3}/k_{3app}, which is equivalent to the ratio of the y-intercept/slope from the linear fit of the data plotted as in Fig. 7(A inset). The above analysis unequivocally proves that inhibition by AMPQD conforms to the classical slow-onset tight-binding reversible inhibition.

When the time-dependent inhibition data for PQD were analyzed, it was clear that the inhibition can be merely classified as classical tight-binding reversible inhibition because the curves show no hint of biphasic nonlinearity even at high inhibitor concentrations (Fig. 7C). Because PQD is the parent molecule of AMPQD, the slow-onset behavior of the latter compound implicates 4-aminophenyl methyl substitution at the seventh position. It should also be noted that, unlike the inhibition mode of PQD, AMPQD inhibition of the enzyme is similar to that shown by MTX (Fig. 7D). However, the physical basis for the slow-onset behavior of both AMPQD and MTX in DHFRs remains unexplained, and we propose that substitutions on the 7H-pyrrolo [3,2-*f*] quinazoline-1,3-diamine for AMPQD and 2,4-diaminopteridin on MTX might be the principal determinant of the slow-onset behavior.

Differential inhibition of human and *E. coli* DHFR

Escherichia coli and human DHFR share 28% sequence identity and are structurally highly conserved (Fig. S5). It is well demonstrated that inhibitors designed against prokaryotic DHFRs inhibit the activity of DHFRs from eukaryotic sources, given the high sequence and structural similarity of this protein across different evolutionary lineages [2]. There are several examples of such broad inhibition with the most prominent example being the commonly employed antifolate MTX, which is known to inhibit DHFRs from *E. coli*, rat and *Plasmodium* species [2]. However, differences in potency and mode of inhibition, and the fact that antifolates target only rapidly

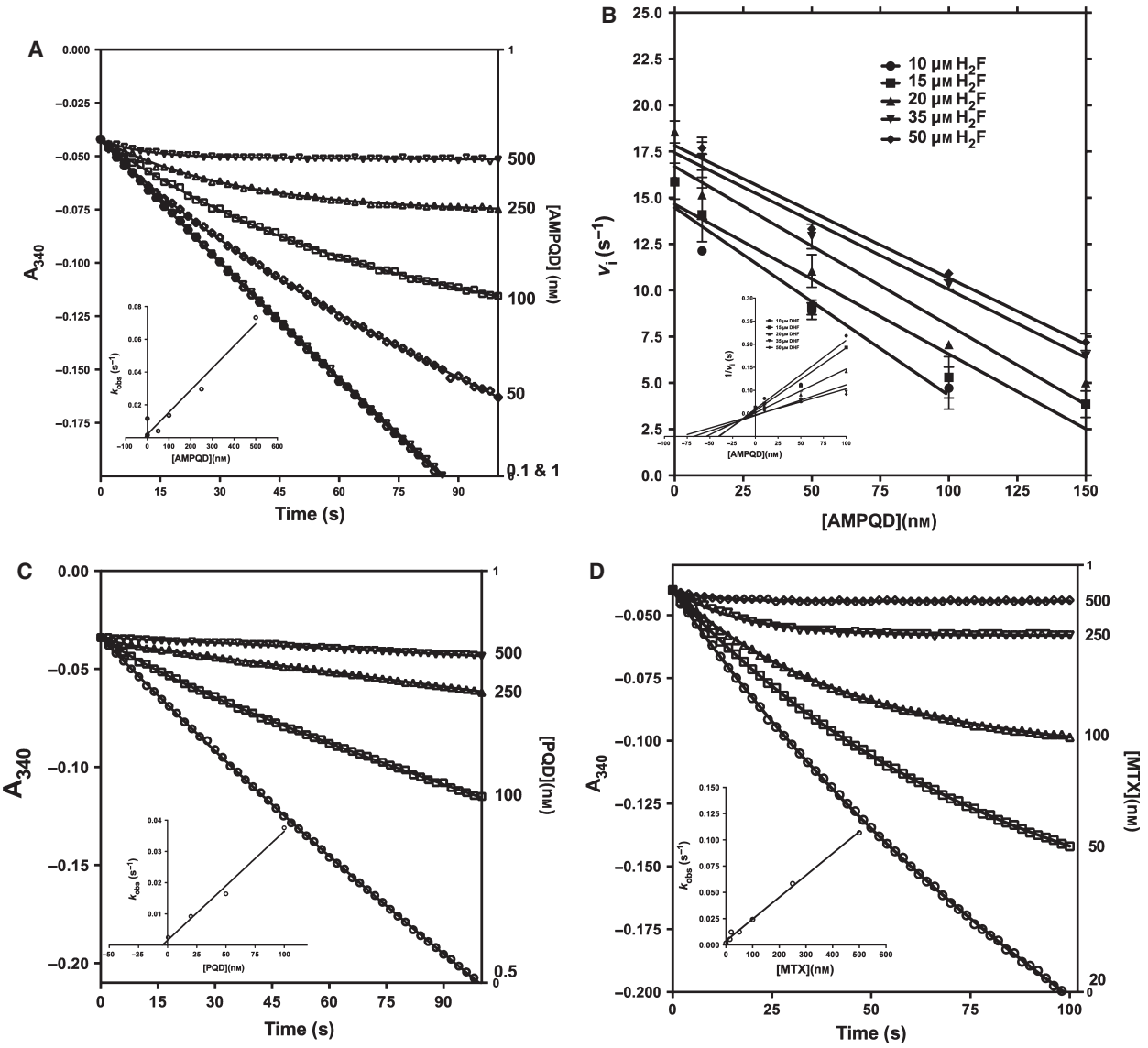

Fig. 7. (A) Time-dependent inactivation of *E. coli* DHFR by 0–500 nM AMPQD. (Inset) k_{obs} plotted as a function of [AMPQD]. (B) Direct plot for the effect of AMPQD on the initial velocity of H_2F reduction of DHFR at various substrate concentrations. (Inset) Linearized plot of the data in (B). (C) Time-dependent inactivation of *E. coli* DHFR by 0–500 nM PQD. (Inset) k_{obs} plotted as a function of [PQD]. (D) Time-dependent inactivation of *E. coli* DHFR by 0–500 nM MTX. (Inset) k_{obs} plotted as a function of [MTX]. The solid curves represent the best fit of the data to Eqn (7) for slow binding inhibition using GraphPad PRISM v. 6.0e.

proliferating cells like pathogenic microbes and tumors enable selective employment of them for specific treatment goals. With this aim, the hits obtained from the FINDSITE^{comb} study [15] were assessed for their inhibitory activity on human DHFR. Figure 1 shows the comparative histogram of inhibition, demonstrating that both human and *E. coli* DHFR are inhibited to similar extent by various inhibitors at 1 mM inhibitor concentration. To understand the inhibition further, the IC_{50} values for the various molecules were estimated (Table 1 and Figs 2A, S2). Marked differences in the potency of AMPQD and PQD were seen in their inhibition of the homologous proteins from humans and *E. coli*. AMPQD, the novel hit from our study, showed an IC_{50} of 599.0 ± 7.2 nM for the human DHFR, which is approximately threefold less potent than the IC_{50} for *E. coli* DHFR (Fig. 2A and Table 1). The most dramatic difference was PQD's inhibition of human DHFR with an IC_{50} value of 3.09 ± 0.17 μM, representing a 30-fold reduction in the

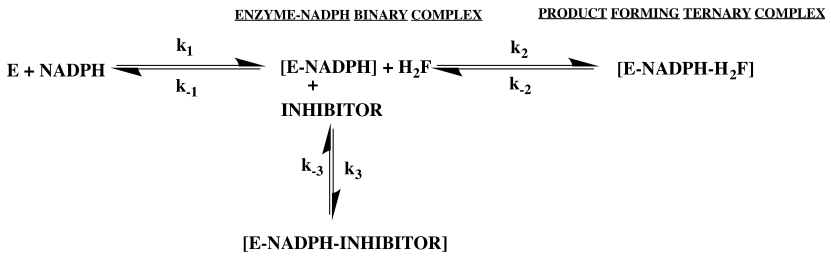

Scheme 1. Kinetic scheme for inhibitor binding to *E. coli* DHFR.

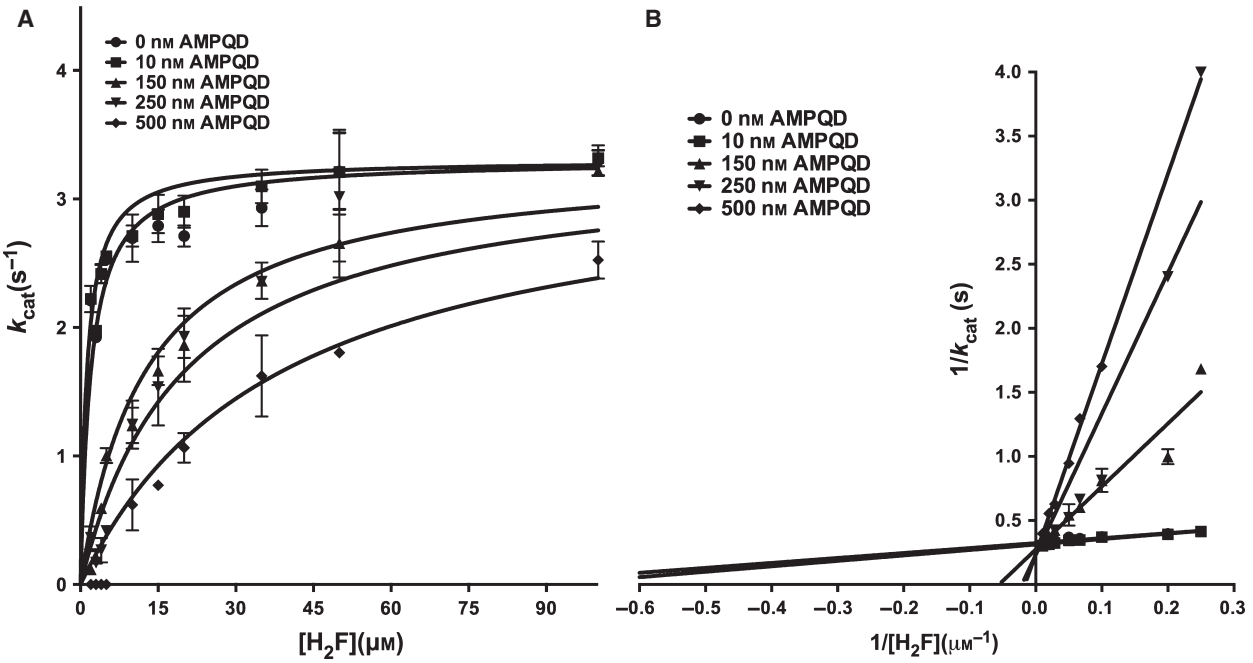

Fig. 8. Inhibition kinetics of AMPQD (NSC309401) for human DHFR. (A) Fit of the primary data to the competitive inhibition model for H_2F titration at several fixed concentrations of AMPQD. (B) Double-reciprocal Lineweaver–Burk plot of H_2F titration at several fixed concentrations of AMPQD. The *y*-axis shows the k_{cat} value. The experimental data points were fit to the model using the nonlinear curve-fitting algorithm of GraphPad PRISM v. 6.0e.

potency of inhibition vis-à-vis *E. coli* DHFR (Fig. S2A and Table 1). However, the IC_{50} values for inhibition of human and *E. coli* DHFR by MTX were comparable, with a value of ~ 148 nM for the former and ~ 152 nM for the latter. For the remaining molecules, the parameters are summarized in Table 1 and Fig. S2(B,C).

In order to further assess the effect of AMPQD on the human enzyme, competition experiments were performed by titrating H_2F at several fixed concentrations of AMPQD. The curves thus obtained were fit to various inhibition models with the best fit obtained for competitive inhibition (Fig. 8A). Further, the double-reciprocal Lineweaver–Burk plot shows intersection of the lines on the *y*-axis, reinforcing the competitive inhibition (Fig. 8B). This indicates that AMPQD inhibits the human enzyme by competitive displacement of substrate H_2F, similar to its mode of action against the *E. coli* enzyme. However, the K_i value of 22.47 ± 3.66 nM for the human enzyme is almost threefold higher than that obtained for the *E. coli* enzyme (7.4 nM), indicative of poorer inhibition of the former.

Furthermore, upon analyzing the time dependence of NADPH depletion in the presence of AMPQD for the human enzyme, no nonlinearity was evident. This is indicative of neither slow onset nor slow dissociation of the inhibitor molecule to the human enzyme (Fig. S6A). This is unlike the behavior displayed by the inhibitor AMPQD on the *E. coli* enzyme where prominent nonlinearity was evident from the time-

course of NADPH depletion in the presence of the inhibitor (Fig. 7A). Likewise, PQD also did not show any slow-onset of inhibition on the human enzyme, exactly mirroring its behavior on *E. coli* DHFR (Fig. S6B and 7B). The differences in the mode of inhibition by AMPQD of the human and *E. coli* enzyme are strongly indicative of differences in the binding site microenvironment between the two homologs. In fact, a study by Bhabha *et al.* [24] has shown that, despite high structural similarity, the dynamics of the active site loop movements varies substantially between human and *E. coli* DHFR. This, they hypothesize, results in markedly different inhibition by the product $NADP^+$ of the two homologs (IC_{50} of ~ 620 μM for human DHFR versus ~ 5 mM for *E. coli* DHFR). However, inhibition of human DHFR by the known antifolate MTX shows signs of pronounced nonlinearity in the time-course curves of NADPH consumption, indicating that the inhibitor retains its slow-onset behavior as seen with *E. coli* DHFR (Fig. S6C). Moreover, the plot of k_{obs} versus MTX concentration is hyperbolic, indicative of isomerization after inhibitor binding (Fig. S6D). This is yet another behavior seen in the inhibition of the human enzyme that is markedly different from that shown for its *E. coli* counterpart whereby, in the case of the latter, there was no isomerization whatsoever as seen in the linear k_{obs} versus [MTX] plot for the inhibitor concentrations tested. (insets of Fig. 7D).

Discussion

Because DHFR is a pivotal enzyme in the synthesis of precursors of DNA, it has been the target for both anticancer and antibacterial drugs [2]. There has been a plethora of folate analogues that have been synthesized and tested for potential inhibitory activity against DHFRs from various sources [2,25]. Principal among these are MTX, used prevalently as an anticancer drug, and trimethoprim, used as an antibacterial drug. In spite of multiple inhibitors designed against DHFRs from various organisms, detailed mechanistic characterization is available for only a few of these molecules. However, detailed kinetic characterization of an inhibitor is essential for designing efficient inhibitors with greater potency against the intended target, determining the proper dose for testing on cellular/animal disease models and understanding the pharmacodynamics. Further, because DHFR acquires rapid resistance to newly discovered antifolates, it is necessary to keep discovering novel small molecules that inhibit this enzyme, especially given the rise in instances of nosocomial *E. coli* infections in hospitalized patients. Several reports in the literature highlight the fact that the incidence of *E. coli*-mediated infections in hospitalized patients is on the rise, with one study showing multi-drug-resistant *E. coli* as the causative agent of urinary tract infection responsible for 40–50% of total nosocomial infections [7,26,27,28]. Our study shows that AMPQD, a novel 7H-pyrrolo [3,2-*f*] quinazoline-1,3-diamine, is a potent inhibitor of the bacterial enzyme. Further, it also shows that compounds NSC80735, NSC55152 and NSC123458 show reasonable inhibition, with μM IC_{50} values, and represent scaffolds amenable to modifications for the development of novel DHFR inhibitors. Whereas NSC80735 and NSC55152 contain concatenated nitrophenyl and aminophenyl groups, NSC123458 is a dibenzazepine that is a common structural scaffold in many antidepressants and analgesics.

In the current study, detailed steady-state inhibition experiments on *E. coli* DHFR have shown that the small molecules AMPQD and PQD bind to the H_2F-binding site and prefer the NADPH-bound binary form of the enzyme. This hints at sequential binding of the substrates NADPH followed by H_2F, given that the small molecules are structural analogues of H_2F. This order of substrate and substrate analogue binding is in conformity with those proposed in the literature [4]. Further, it is well documented in the literature that NADPH exerts a synergistic effect on folate analogues binding to DHFR. NADPH enhances the binding of all the classical (phenyltriazine, DADMP) and slow-binding (MTX, trimethoprim) inhibitors of DHFR, although it has no effect on either pyrimethamine or folate binding to DHFR. It has been reported that the degree of NADPH synergism can vary as much as 1000-fold for the binding among the different folate analogues [29]. We posit that because NADP and NADPH are present in equal concentrations in the prokaryotic cytosol (as opposed to the eukaryotic cytosol where NADP is no more than 1% of the concentration of NADPH) [30], for an inhibitor to be an effective drug, it might be advantageous for it to inhibit the product-forming ternary form of the enzyme. Hence, inhibitors showing greater synergy may be preferable as potential lead candidates.

Tight-binding inhibitors are an important class in which the affinity of the inhibitor for its cognate enzyme is so high that the equilibrium assumptions employed to compute the affinity of the inhibitor for the enzyme no longer remain valid. Further, a lot of well-known inhibitors extensively employed as drugs also display the property of slow-onset of inhibition because of the time-dependent establishment of equilibrium between the enzyme-bound form and free

inhibitor. A few examples are captopril [31], an angiotensin inhibitor, Dup697 [32], a COX2 inhibitor, and MTX [22,33], a DHFR inhibitor. MTX inhibits DHFR in a time-dependent manner involving the rapid formation of an enzyme–NADPH–MTX complex that undergoes relatively slow, reversible isomerization to form a thermodynamically stable ternary enzyme complex resulting in enhanced inhibition. Hence, the MTX concentration required for inhibition is comparable with the enzyme concentration employed in steady-state kinetic studies. This type of inhibition is categorized as slow-on/slow-off tight-binding inhibition [22]. Other folate analogues that exhibit slow-onset, tight-binding inhibition are 5-deazamethotrexate, aminopterin and trimethoprim, although the extent to which they bring about isomerization for slow dissociation differs significantly. Here, we demonstrate that AMPQD shows a slow-onset tight-binding behavior similar to that shown by MTX. However, upon analyzing the time-dependent inhibition curves, it becomes obvious that there is no pronounced isomerization, if any, which could be detected in the concentration range of inhibitor assessed. Mainly, the k_{obs} versus inhibitor plots were linear both for AMPQD and MTX (Fig. 7A,D) even at high inhibitor concentrations. Further, we could convincingly rule out the possibility that there is isomerization of the enzyme between two different forms with the inhibitor preferably binding to one form by the fact that k_{obs} increased (rather than decreased) with increasing inhibitor. For DHFR from *E. coli*, it has been reported that all folate analogues that act as tight binding inhibitors exhibit slow binding characteristics. However, slow-onset does occur without tight binding as observed with 5-deazafolate. To the best of our knowledge, for the first time, we show that PQD is a tight-binding inhibitor of DHFR not displaying any slow-binding behavior, as is evident from the linear time-course curves (Fig. 7B).

Further, pronounced differences in the potency of inhibition of AMPQD and PQD for the human and *E. coli* homologue, with an order-of-magnitude higher affinity for the latter, makes these molecules good candidates for development as effective antibiotics. It has been shown in the literature that recombinantly expressed human DHFR cannot complement DHFR-deficient *E. coli* cells, and this was ascribed to differences in the dynamics and conformational plasticity of the active site loops across the two different DHFRs [24]. This conjecture is further validated by our studies showing similar site of binding on both human and *E. coli* DHFR for the inhibitor AMPQD (H_2F-binding site) (see Figs 4A and 8A) albeit with different modes (slow-onset tight binding for the *E. coli* enzyme, but merely tight binding for the human homologue as in Figs 7A and S6A). Further, the isomerization of MTX after initial binding on the human enzyme, as evident in the nonlinearity of k_{obs} versus MTX plot (Fig. S6D), is completely absent from its binding to the *E. coli* DHFR (Fig. 7D inset).

In conclusion, employing detailed inhibition kinetics, this study reports a set of novel and potent inhibitors of prokaryotic DHFR that have the potential to be developed as antibiotics for amelioration of conditions arising from bacterial infections. This, combined with the already reported antibacterial activity of AMPQD against two different strains of *E. coli* (multidrug-resistant *E. coli* and DH5α), a strain of methicillin-resistant *S. aureus* and a strain of vancomycin-resistant *Enterococcus faecalis*, makes this molecule a potential candidate for development as an antibiotic. Further, detailed kinetic assessment of the inhibition brought about by this molecule shows that it is competitive with respect to H_2F and uncompetitive with respect to NADPH, with a preference of the inhibitor molecule for the NADPH-bound form of the enzyme. Furthermore, we show that although AMPQD is a slow-onset tight-binding inhibitor of *E. coli* DHFR, similar to MTX, PQD is merely a tight-binding inhibitor with no slow-onset behavior. This detailed kinetic characterization of the inhibitors, by means of providing additional insight on the structure–activity relationship, paves the way for development of better antifolates.

Experimental procedures

Reagents

All reagents and chemicals, unless mentioned otherwise, were of high quality and were procured from Sigma-Aldrich Co., (St. Louis, MO, USA), Amresco (Solon, OH, USA), or Fisher Scientific (Waltham, MA, USA). *Escherichia coli* dihydrofolate reductase was provided by E. Shakhnovich (Harvard University, Cambridge, MA, USA). The small-molecule AMPQD (NSC309401), MTX (NSC740), PQD (NSC339578), methylbezoprim (NSC382035), pralatrexate (NSC754230), pemetrexed (NSC698037), 6,7-bis(4-aminophenyl) pteridine-2,4-diamine (NSC61642), 2,2′-iminostilbene (NSC123458), benzoylpas (NSC159686), cibanaphthol RPH (NSC50690), NSC80735, NSC157522 and NSC55152 were provided by the Developmental Therapeutics Program (DTP) of the National Cancer Institute (NCI), National Institutes of Health (NIH, Bethesda, MD, USA). Dihydrofolate reductase assay kit (CS0340) was obtained from Sigma-Aldrich and contained 0.1 units of human DHFR (D6566), dihydrofolic acid, MTX and NADPH.

Dihydrofolate reductase assay

The stock solutions of H_2F and NADPH were reconstituted as per the manufacturer's instructions. DHFR catalyzes the transfer of a hydride from NADPH to H_2F with an accompanying protonation to produce H_4F. Overall, H_2F is reduced to H_4F and NADPH is oxidized to $NADP^+$, resulting in a net decrease in the absorbance of NADPH at 340 nm. To understand the kinetics of *E. coli* DHFR and human DHFR, the rate of reduction of H_2F to H_4F was monitored by the decrease in absorbance at 340 nm for 100 s. The amount of product formed from the slope of initial velocity curves was computed using a molar extinction coefficient (ε) of 6.2×10^3 $M^{-1}{\cdot}cm^{-1}$ for β-NADPH at 340 nm [34]. The nonenzymatic hydrolysis of NADPH was normalized by monitoring the reaction in a double beam Hitachi U-2010 UV/vis spectrophotometer (Hitachi High Technologies America, Inc., San Jose, CA, USA) with an appropriate blank. All assays were carried out in the linear range of enzyme concentration. Assays were initiated with the addition of enzyme to the sample cuvette after zeroing the absorbance reading with respect to the reference cuvette. The initial velocities, where product formation was < 5%, were measured for reaction mixtures containing 100 mM Hepes pH 7.3 at room temperature (~ 22 °C).

To determine the K_m and V_{max} for H_2F and NADPH, the respective substrate was titrated at fixed saturating concentration of the other, and the resultant velocities were plotted against substrate concentration and fit to Eqn (1) for one-site binding hyperbola

$$d[P]/dt = (V_{max} \times [S])/(K_m + [S]) \quad (1)$$

where $d[P]/dt$ is the rate of product formation, V_{max} is the maximum velocity, $[S]$ is the substrate concentration and K_m is the Michaelis–Menten constant for the substrate assayed.

All measurements were performed in duplicate, and the error values indicated are standard deviations (SD). The concentration of *E. coli* DHFR used was 16.7 nM (see below for protocol of enzyme concentration estimation). Unless mentioned otherwise, all data were fit using nonlinear curve fitting subroutines of GraphPad PRISM, v. 4.0 (GraphPad Software, Inc., San Diego, CA, USA).

Velocity–titration curves for enzyme concentration estimation

To interpret inhibition data without errors (see below), an accurate estimate of catalytically active $[E_t]$ is essential. Methods suggested by Williams *et al.* [33], whereby velocity measurements after preincubation with a ligand (where enzyme–ligand complex is inactive and dissociates slowly), were followed to estimate the catalytically active total enzyme concentration. Briefly, 0.1 μg of *E. coli* DHFR and 0.16 μg of human DHFR were preincubated with various concentrations of MTX in 100 mM Hepes pH 7.3 and 60 μM NADPH for 300 s. The reaction was initiated with 50 μM H_2F, and the resultant velocity was plotted as a function of MTX concentration (Fig. S7A–D). The total concentration of the catalytically active enzyme is given by the intercept of the curve with the abscissa, which corresponds to 16.7 nM for of *E. coli* DHFR and 12.4 nM for human DHFR. The experiment was repeated with a preincubation time of 600 s, giving identical results. The concentration was also estimated employing a molar extinction coefficient of 33 460 $M^{-1}{\cdot}cm^{-1}$ for *E. coli* DHFR and 25 440 $M^{-1}{\cdot}cm^{-1}$ for the human enzyme at 280 nm.

Inhibition kinetics

Various inhibitors were assessed for their inhibitory effect on the dihydrofolic acid reducing ability of *E. coli* DHFR and human DHFR. Initial inhibition was assessed in a reaction mixture containing 100 mM Hepes pH 7.3, 60 μM NADPH, 50 μM H_2F and 1 mM of each inhibitor. The assay mix contained 16.7 nM of *E. coli* DHFR and 12.4 nM of human DHFR. Subsequently, both the potency of the inhibitor and its affinity for the enzyme were computed by experimental IC_{50} determination and competition assays to determine its K_i. IC_{50} determination assays were carried out in 100 mM Hepes pH 7.3, 60 μM NADPH, 50 μM H_2F and variable concentration of each inhibitor. The enzyme concentration was as specified above. The curves were fit to Eqn (2), where I is the inhibitor concentration, and y is the percentage activity.

$$y = 100\%/[1 + (I/IC_{50})] \quad (2)$$

Furthermore, K_{iapp} values were computed from the IC_{50} curves by fitting them to the quadratic Morrison equation (Eqn 3) for tight-binding inhibition. This equation accounts for tight binding by doing away with the assumption that the free concentration of inhibitor equals the total concentration.

$$v_i/v_0 = 1 - (([E]_T + [I]_T + K_{iapp}) - (\sqrt{([E]_T + [I]_T + K_{iapp})^2 - 4[E]_T[I]_T}))/2[E]_T \quad (3)$$

where v_i is the velocity in the presence of inhibitor, v_0 is the velocity in the absence of inhibitor, $[E]_T$ is the total enzyme, $[I]_T$ is the total inhibitor and K_{iapp} is the apparent K_i.

Experimental K_i value determinations were carried out by titrating the substrates H_2F and NADPH, around their respective K_m values, at various fixed concentrations of the inhibitors. The resulting [substrate] versus velocity curves were fit to the models of competitive inhibition (Eqn 4),

noncompetitive inhibition (Eqn 5) and uncompetitive inhibition (Eqn 6) in order to discriminate between the different types of inhibition and to estimate the various inhibition constants (K_i).

Competitive:

$$v = V_{max}[S]/\{K_m(1 + [I]/K_i) + [S]\} \quad (4)$$

Non-competitive:

$$v = V_{max}[S]/\{K_m(1 + [I]/K_i) + [S](1 + [I]/K_i)\} \quad (5)$$

Uncompetitive:

$$v = V_{max}[S]/\{K_m + [S](1 + [I]/K_i)\} \quad (6)$$

where v is the velocity of the reaction, V_{max} is the maximum velocity, $[S]$ is the substrate concentration and $[I]$ is the inhibitor concentration. K_m is the Michaelis–Menten constant, and K_i is the inhibition constant. Visual assessment of the type of inhibition was undertaken by plotting the double reciprocal Lineweaver–Burk plot from experimental data points constituting the primary plot.

Progress curve analysis: slow–tight binding

The slow-onset inhibition of *E. coli* and human DHFR brought about by AMPQD, PQD and MTX was monitored by initiating the reaction with 16.7 nM of *E. coli* DHFR and 12.4 nM of human DHFR in assay mixtures containing 100 mM Hepes pH 7.3, 50 μM H_2F, 60 μM NADPH and varying concentrations of inhibitor (0–25 μM). The reactions were allowed to proceed until the progress curve became linear, indicating that the enzyme has attained a steady state. To ensure that substrate depletion does not significantly affect the reaction rate, substrate concentrations greater than 10 times the respective K_m values were used. Progress curves were analyzed as described previously [35]. Briefly, the resulting progress curves were fit to the integrated rate equation (Eqn 7) for slow binding inhibition by nonlinear regression analysis.

$$A_t = A_0 - v_s \times t - (v_i - v_s)(1 - \exp(-k_{obs} \times t))/k_{obs} \quad (7)$$

where, A_t and A_0 are the absorbance at time t and time 0, k_{obs} is the pseudo-first-order rate constant for approach to the steady state, whereas v_i and v_s correspond to the initial and final slopes of the progress curve. Values for v_i, v_s and k_{obs} were obtained at each inhibitor concentration. Progress curves were approximately linear in the absence of added inhibitor. The values of k_{obs}, v_i and v_s obtained from the fit to Eqn (7) were replotted to obtain the k_{off} and k_{on} for inhibitor binding for a classical single-step inhibition mechanism in which rapid reversible binding of the inhibitor occurs to the enzyme.

Further, the patterns were also analyzed for possible two-step inhibition mechanism. In this case, which signifies a second slow step of isomerization after inhibitor binding to form the final enzyme–inhibitor complex, the following equation was used to fit the replot of k_{obs} versus inhibitor to gauge its nonlinearity.

$$k_{obs} = k_{-4} + k_4[I]/(K_{app-1} + [I]) \quad (8)$$

where k_4 and k_{-4} represent the forward and reverse rate constants for the isomerization step.

Thermal shift assay methodology

High-throughput thermal-shift assays were carried out following established guidelines [36,37]. Briefly, thermal melt curves for proteins were obtained from samples aliquoted in 96–well plates using a RealPlex quantitative PCR instrument from Eppendorf (Hauppauge, NY, USA) with 5 × Sypro orange dye as the fluorescent probe (Invitrogen, Carlsbad, CA, USA). (λ_{ex} is 465 nm and λ_{em} is 580 nm). A heating gradient of 1 °C·min^{-1} from 25 to 75 °C was used. Thermal melt experiments were carried out in 100 mM Hepes pH 7.3 and 150 mM NaCl with 20 μL total volume of the reaction mix. The concentration of AMPQD was varied from 0 to 500 nM at 5 μM of *E. coli* DHFR. All experiments were performed in duplicate, with the mean value considered for further analysis.

The curves were fit to Boltzmann's equation (Eqn 9) for estimating the T_m (melting temperature) from the observed intensity of fluorescence, I.

$$I = I_{min} + ([I_{max} - I_{min}]/(1 + e^{((Tm-T)/a)}) \quad (9)$$

I_{min} and I_{max} are the minimum and maximum intensities, and a is the slope of the curve at the transition midpoint temperate, T_m [36]. Thermodynamic parameters were estimated as specified in the previous literature [15].

Acknowledgements

This project was funded by GM-37408 and GM-48835 of the Division of General Medical Sciences of the NIH. The authors wish to thank Prof. Eugene Shakhnovich, Harvard University, for providing purified *E. coli* DHFR protein. We would also like to thank the Developmental Therapeutics Program of the National Cancer Institute for providing the small molecules used in this study.

Author contributions

BS conceived of the study, participated in its design, carried out the experiments, analyzed and interpreted the results, and drafted the manuscript. JS conceived of the study, participated in its design and coordination, provided appropriate resources, helped analyze

the data, and was involved in drafting and critically reviewing the manuscript. All authors read and approved the final manuscript.

References

1 Liu CT, Francis K, Layfield JP, Huang X, Hammes-Schiffer S, Kohen A & Benkovic SJ (2014) *Escherichia coli* dihydrofolate reductase catalyzed proton and hydride transfers: temporal order and the roles of Asp27 and Tyr100. *Proc Natl Acad Sci USA* **111**, 18231–18236.

2 Schweitzer BI, Dicker AP & Bertino JR (1990) Dihydrofolate reductase as a therapeutic target. *FASEB J* **4**, 2441–2452.

3 Sawaya MR & Kraut J (1997) Loop and subdomain movements in the mechanism of *Escherichia coli* dihydrofolate reductase: crystallographic evidence. *Biochemistry* **36**, 586–603.

4 Fierke CA, Johnson KA & Benkovic SJ (1987) Construction and evaluation of the kinetic scheme associated with dihydrofolate reductase from *Escherichia coli*. *Biochemistry* **26**, 4085–4092.

5 Cayley PJ, Dunn SM & King RW (1981) Kinetics of substrate, coenzyme, and inhibitor binding to *Escherichia coli* dihydrofolate reductase. *Biochemistry* **20**, 874–879.

6 Stone SR & Morrison JF (1982) Kinetic mechanism of the reaction catalyzed by dihydrofolate reductase from *Escherichia coli*. *Biochemistry* **21**, 3757–3765.

7 Bean DC, Krahe D & Wareham DW (2008) Antimicrobial resistance in community and nosocomial *Escherichia coli* urinary tract isolates, London 2005–2006. *Ann Clin Microbiol Antimicrob* **7**, 13.

8 Borst P & Ouellette M (1995) New mechanisms of drug resistance in parasitic protozoa. *Annu Rev Microbiol* **49**, 427–460.

9 Gonen N & Assaraf YG (2012) Antifolates in cancer therapy: structure, activity and mechanisms of drug resistance. *Drug Resist Updat* **15**, 183–210.

10 Hagner N & Joerger M (2010) Cancer chemotherapy: targeting folic acid synthesis. *Cancer Manag Res* **2**, 293–301.

11 Chio LC & Queener SF (1993) Identification of highly potent and selective inhibitors of *Toxoplasma gondii* dihydrofolate reductase. *Antimicrob Agents Chemother* **37**, 1914–1923.

12 Guan J, Zhang Q, O'Neil M, Obaldia N 3rd, Ager A, Gerena L & Lin AJ (2005) Antimalarial activities of new pyrrolo [3,2-f]quinazoline-1,3-diamine derivatives. *Antimicrob Agents Chemother* **49**, 4928–4933.

13 Kuyper LF, Baccanari DP, Jones ML, Hunter RN, Tansik RL, Joyner SS, Boytos CM, Rudolph SK, Knick V, Wilson HR *et al*. (1996) High-affinity inhibitors of dihydrofolate reductase: antimicrobial and anticancer activities of 7,8-dialkyl-1,3-diaminopyrrolo [3,2-f]quinazolines with small molecular size. *J Med Chem* **39**, 892–903.

14 Zolli-Juran M, Cechetto JD, Hartlen R, Daigle DM & Brown ED (2003) High throughput screening identifies novel inhibitors of *Escherichia coli* dihydrofolate reductase that are competitive with dihydrofolate. *Bioorg Med Chem Lett* **13**, 2493–2496.

15 Srinivasan B, Zhou H, Kubanek J & Skolnick J (2014) Experimental validation of FINDSITE(comb) virtual ligand screening results for eight proteins yields novel nanomolar and micromolar binders. *J Cheminform* **6**, 16.

16 Srinivasan B, Skolnick J & Zhou H (2014) Molecules with potent DHFR binding affinity and antibacterial activity. (USPTO, ed.). Georgia Tech Research Corporation, Atlanta, GA.

17 Murakami C, Ohmae E, Tate S, Gekko K, Nakasone K & Kato C (2010) Cloning and characterization of dihydrofolate reductases from deep-sea bacteria. *J Biochem* **147**, 591–599.

18 Stone SR & Morrison JF (1988) Dihydrofolate reductase from *Escherichia coli*: the kinetic mechanism with NADPH and reduced acetylpyridine adenine dinucleotide phosphate as substrates. *Biochemistry* **27**, 5493–5499.

19 Cha S (1975) Tight-binding inhibitors-I. *Kinetic Behav Biochem Pharmacol* **24**, 2177–2185.

20 Morrison JF (1969) Kinetics of the reversible inhibition of enzyme-catalysed reactions by tight-binding inhibitors. *Biochim Biophys Acta* **185**, 269–286.

21 Williams JW & Morrison JF (1979) The kinetics of reversible tight-binding inhibition. *Methods Enzymol* **63**, 437–467.

22 Stone SR, Montgomery JA & Morrison JF (1984) Inhibition of dihydrofolate reductase from bacterial and vertebrate sources by folate, aminopterin, methotrexate and their 5-deaza analogues. *Biochem Pharmacol* **33**, 175–179.

23 Tahar R, de Pecoulas PE, Basco LK, Chiadmi M & Mazabraud A (2001) Kinetic properties of dihydrofolate reductase from wild-type and mutant *Plasmodium vivax* expressed in *Escherichia coli*. *Mol Biochem Parasitol* **113**, 241–249.

24 Bhabha G, Ekiert DC, Jennewein M, Zmasek CM, Tuttle LM, Kroon G, Dyson HJ, Godzik A, Wilson IA & Wright PE (2013) Divergent evolution of protein conformational dynamics in dihydrofolate reductase. *Nat Struct Mol Biol* **20**, 1243–1249.

25 Abraham A, McGuire JJ, Galivan J, Nimec Z, Kisliuk RL, Gaumont Y & Nair MG (1991) Folate analogues. 34. Synthesis and antitumor activity of non-polyglutamylatable inhibitors of dihydrofolate reductase. *J Med Chem* **34**, 222–227.

26 Schaberg DR, Culver DH & Gaynes RP (1991) Major trends in the microbial etiology of nosocomial infection. *Am J Med* **91**, 72S–75S.
27 Caini S, Hajdu A, Kurcz A & Borocz K (2013) Hospital-acquired infections due to multidrug-resistant organisms in Hungary, 2005–2010. *Euro Surv: Bulletin Europeen sur les Maladies Transmissibles = European Communicable Disease Bulletin*. **18**, 20352–20360.
28 Hassan SA, Jamal SA & Kamal M (2011) Occurence of multidrug resistant and ESBL producing *E. coli* causing urinary tract infections. *J Basic Appl Sci* **7**, 39–43.
29 Stone SR & Morrison JF (1986) Mechanism of inhibition of dihydrofolate reductases from bacterial and vertebrate sources by various classes of folate analogues. *Biochim Biophys Acta* **869**, 275–285.
30 Appleman JR, Beard WA, Delcamp TJ, Prendergast NJ, Freisheim JH & Blakley RL (1990) Unusual transient- and steady-state kinetic behavior is predicted by the kinetic scheme operational for recombinant human dihydrofolate reductase. *J Biol Chem* **265**, 2740–2748.
31 Baudin B & Beneteau-Burnat B (1999) Mixed-type inhibition of pulmonary angiotensin I-converting enzyme by captopril, enalaprilat and ramiprilat. *J Enzym Inhib* **14**, 447–456.
32 Dannhardt G & Kiefer W (2001) Cyclooxygenase inhibitors–current status and future prospects. *Eur J Med Chem* **36**, 109–126.
33 Williams JW, Morrison JF & Duggleby RG (1979) Methotrexate, a high-affinity pseudosubstrate of dihydrofolate reductase. *Biochemistry* **18**, 2567–2573.
34 Horecker BL & Kornberg A (1948) The extinction coefficients of the reduced band of pyridine nucleotides. *J Biol Chem* **175**, 385–390.
35 Rawat R, Whitty A & Tonge PJ (2003) The isoniazid-NAD adduct is a slow, tight-binding inhibitor of InhA, the Mycobacterium tuberculosis enoyl reductase: adduct affinity and drug resistance. *Proc Natl Acad Sci USA* **100**, 13881–13886.
36 Niesen FH, Berglund H & Vedadi M (2007) The use of differential scanning fluorimetry to detect ligand interactions that promote protein stability. *Nat Protoc* **2**, 2212–2221.
37 Crowther GJ, He P, Rodenbough PP, Thomas AP, Kovzun KV, Leibly DJ, Bhandari J, Castaneda LJ, Hol WG, Gelb MH et al. (2010) Use of thermal melt curves to assess the quality of enzyme preparations. *Anal Biochem* **399**, 268–275.

Supporting information

Additional supporting information may be found in the online version of this article at the publisher's web site:

Fig. S1. Kinetic parameters of *E. coli* DHFR for its substrates.

Fig. S2. Curves to determine the IC_{50} values for a select set of small molecules identified in our study.

Fig. S3. MTX–NADPH inhibition kinetics for *E. coli* DHFR.

Fig. S4. Thermal shift assay curves for *E. coli* DHFR at varying concentrations of the inhibitor AMPQD.

Fig. S5. Comparison between *E. coli* and human DHFR.

Fig. S6. Time course analysis for human DHFR inhibition.

Fig. S7. Enzyme concentration estimation by velocity–titration curve method.

Table S1. Kinetic parameters for *E. coli* DHFR.